

Track reconstruction and matching between emulsion and silicon pixel detectors for the SHiP-charm experiment



The SHiP Collaboration

C. Ahdida,⁴⁵ A. Akmete,⁴⁹ R. Albanese,^{15,d,h} J. Alt,⁷ A. Alexandrov,^{15,33,35,d} A. Anokhina,⁴⁰
 S. Aoki,¹⁹ G. Arduini,⁴⁵ E. Atkin,³⁹ N. Azorskiy,³⁰ J.J. Back,⁵⁵ A. Bagulya,³³
 F. Baaltasar Dos Santos,⁴⁵ A. Baranov,⁴¹ F. Bardou,⁴⁵ G.J. Barker,⁵⁵ M. Battistin,⁴⁵
 J. Bauche,⁴⁵ A. Bay,⁴⁷ V. Bayliss,⁵² G. Bencivenni,¹⁶ A.Y. Berdnikov,³⁸ Y.A. Berdnikov,³⁸
 M. Bertani,¹⁶ C. Betancourt,⁴⁸ I. Bezshyiko,⁴⁸ O. Bezshyyko,⁵⁶ D. Bick,⁸ S. Bieschke,⁸
 A. Blanco,²⁹ J. Boehm,⁵² M. Bogomilov,¹ I. Boiarska,³ K. Bondarenko,^{28,58} W.M. Bonivento,¹⁴
 J. Borburgh,⁴⁵ A. Boyarsky,^{28,56} R. Brenner,⁴⁴ D. Breton,⁴ A. Brignoli,⁶ V. Büscher,¹⁰
 A. Buonaura,⁴⁸ S. Buontempo,¹⁵ S. Cadeddu,¹⁴ A. Calcaterra,¹⁶ M. Calviani,⁴⁵
 M. Campanelli,⁵⁴ M. Casolino,⁴⁵ N. Charitonidis,⁴⁵ P. Chau,¹⁰ J. Chauveau,⁵ A. Chepurinov,⁴⁰
 M. Chernyavskiy,³³ K.-Y. Choi,²⁷ A. Chumakov,² P. Ciambone,¹⁶ V. Cicero,¹³ M. Climescu,¹⁰
 A. Conaboy,⁶ L. Congedo,^{12,a} K. Cornelis,⁴⁵ M. Cristinziani,^{11,*} A. Crupano,^{15,d}
 G.M. Dallavalle,¹³ A. Datwyler,⁴⁸ N. D'Ambrosio,¹⁷ G. D'Appollonio,^{14,c} R. de Asmundis,¹⁵
 J. De Carvalho Saraiva,²⁹ G. De Lellis,^{15,35,45,d} M. de Magistris,^{15,j} A. De Roeck,⁴⁵
 M. De Serio,^{12,a} D. De Simone,⁴⁸ L. Dedenko,⁴⁰ P. Dergachev,³⁵ A. Di Crescenzo,^{15,d}
 L. Di Giulio,⁴⁵ N. Di Marco,¹⁷ C. Dib,² H. Dijkstra,⁴⁵ V. Dmitrenko,³⁹ L.A. Dougherty,⁴⁵
 A. Dolmatov,³⁴ D. Domenici,¹⁶ S. Donskov,³⁶ V. Drohan,⁵⁶ A. Dubreuil,⁴⁶ O. Durhan,⁴⁹
 M. Ehler,⁶ E. Elikkaya,⁴⁹ T. Enik,³⁰ A. Etenko,^{34,39} F. Fabbri,¹³ O. Fedin,³⁷ F. Fedotovs,⁵³
 G. Felici,¹⁶ M. Ferrillo,⁴⁸ M. Ferro-Luzzi,⁴⁵ K. Filippov,³⁹ R.A. Fini,¹² H. Fischer,⁷ P. Fonte,²⁹
 C. Franco,²⁹ M. Fraser,⁴⁵ R. Fresa,^{15,i,h} R. Froeschl,⁴⁵ T. Fukuda,²⁰ G. Galati,^{15,d} J. Gall,⁴⁵
 L. Gatignon,⁴⁵ G. Gavrilo,³⁷ V. Gentile,^{15,d} B. Goddard,⁴⁵ L. Golinka-Bezshyyko,⁵⁶
 A. Golovatiuk,^{15,d} V. Golovtsov,³⁷ D. Golubkov,³¹ A. Golutvin,^{53,35} P. Gorbounov,⁴⁵
 D. Gorbunov,³² S. Gorbunov,³³ V. Gorkavenko,⁵⁶ M. Gorshenkov,³⁵ V. Grachev,³⁹
 A.L. Grandchamp,⁴⁷ E. Graverini,⁴⁷ J.-L. Grenard,⁴⁵ D. Grenier,⁴⁵ V. Grichine,³³

N. Gruzinskii,³⁷ A.M. Guler,⁴⁹ Yu Guz,³⁶ G.J. Haefeli,⁴⁷ C. Hagner,⁸ H. Hakobyan,² I.W. Harris,⁴⁷ E. van Herwijnen,³⁵ C. Hessler,⁴⁵ A. Hollnagel,¹⁰ B. Hosseini,⁵³ M. Hushchyn,⁴¹ G. Iaselli,^{12,a} A. Iuliano,^{15,d} R. Jacobsson,⁴⁵ D. Joković,⁴² M. Jonker,⁴⁵ I. Kadenko,⁵⁶ V. Kain,⁴⁵ B. Kaiser,⁸ C. Kamiscioglu,⁵⁰ D. Karpenkov,³⁵ K. Kershaw,⁴⁵ M. Khabibullin,³² E. Khalikov,⁴⁰ G. Khaustov,³⁶ G. Khoriauli,¹⁰ A. Khotyantsev,³² Y.G. Kim,²⁴ V. Kim,^{37,38} N. Kitagawa,²⁰ J.-W. Ko,²³ K. Kodama,¹⁸ A. Kolesnikov,³⁰ D.I. Kolev,¹ V. Kolosov,³⁶ M. Komatsu,²⁰ A. Kono,²² N. Konovalova,^{33,35} S. Kormannshaus,¹⁰ I. Korol,⁶ I. Korol'ko,³¹ A. Korzenev,⁴⁶ V. Kostyukhin,¹¹ E. Koukovini Platia,⁴⁵ S. Kovalenko,² I. Krasilnikova,³⁵ Y. Kudenko,^{32,39,g} E. Kurbatov,⁴¹ P. Kurbatov,³⁵ V. Kurochka,³² E. Kuznetsova,³⁷ H.M. Lacker,⁶ M. Lamont,⁴⁵ G. Lanfranchi,¹⁶ O. Lantwin,^{48,35} A. Lauria,^{15,d} K.S. Lee,²⁶ K.Y. Lee,²³ N. Leonardo,²⁹ J.-M. Lévy,⁵ V.P. Loschiavo,^{15,h} L. Lopes,²⁹ E. Lopez Sola,⁴⁵ F. Lyons,⁷ V. Lyubovitskij,² J. Maalmi,⁴ A.-M. Magnan,⁵³ V. Maleev,³⁷ A. Malinin,³⁴ Y. Manabe,²⁰ A.K. Managadze,⁴⁰ M. Manfredi,⁴⁵ S. Marsh,⁴⁵ A.M. Marshall,⁵¹ A. Mefodev,³² P. Mermod,⁴⁶ A. Miano,^{15,d} S. Mikado,²¹ Yu. Mikhaylov,³⁶ A. Mikulenko,²⁸ D.A. Milstead,⁴³ O. Mineev,³² A. Montanari,¹³ M.C. Montesi,^{15,d} K. Morishima,²⁰ S. Movchan,³⁰ Y. Muttoni,⁴⁵ N. Naganawa,²⁰ M. Nakamura,²⁰ T. Nakano,²⁰ S. Nasybulin,³⁷ P. Ninin,⁴⁵ A. Nishio,²⁰ B. Obinyakov,³⁴ S. Ogawa,²² N. Okateva,^{33,35} J. Osborne,⁴⁵ M. Ovchynnikov,^{28,56} N. Owtscharenko,^{11,*} P.H. Owen,⁴⁸ P. Pacholek,⁴⁵ A. Paoloni,¹⁶ B.D. Park,²³ A. Pastore,¹² M. Patel,^{53,35} D. Pereyma,³¹ A. Perillo-Marccone,⁴⁵ G.L. Petkov,¹ K. Petridis,⁵¹ A. Petrov,³⁴ D. Podgrudkov,⁴⁰ V. Poliakov,³⁶ N. Polukhina,^{33,35,39} J. Prieto Prieto,⁴⁵ M. Prokudin,³¹ A. Prota,^{15,d} A. Quercia,^{15,d} A. Rademakers,⁴⁵ A. Rakai,⁴⁵ F. Ratnikov,⁴¹ T. Rawlings,⁵² F. Redi,⁴⁷ A. Reghunath,⁶ S. Ricciardi,⁵² M. Rinaldesi,⁴⁵ Volodymyr Rodin,⁵⁶ Viktor Rodin,⁵⁶ P. Robbe,⁴ A.B. Rodrigues Cavalcante,⁴⁷ T. Roganova,⁴⁰ H. Rokujo,²⁰ G. Rosa,^{15,d} T. Rovelli,^{13,b} O. Ruchayskiy,³ T. Ruf,⁴⁵ V. Samoylenko,³⁶ V. Samsonov,³⁹ F. Sanchez Galan,⁴⁵ P. Santos Diaz,⁴⁵ A. Sanz Ull,⁴⁵ A. Saputi,¹⁶ O. Sato,²⁰ E.S. Savchenko,³⁵ J.S. Schliwinski,⁶ W. Schmidt-Parzefall,⁸ M. Schumann,⁷ N. Serra,^{48,35} S. Sgobba,⁴⁵ O. Shadura,⁵⁶ A. Shakin,³⁵ M. Shaposhnikov,⁴⁷ P. Shatalov,^{31,35} T. Shchedrina,^{33,35} L. Shchutska,⁴⁷ V. Shevchenko,^{34,35} H. Shibuya,²² L. Shihora,⁶ S. Shirobokov,⁵³ A. Shustov,³⁹ S.B. Silverstein,⁴³ S. Simone,^{12,a} R. Simoniello,¹⁰ M. Skorokhvatov,^{39,34} S. Smirnov,³⁹ G. Soares,²⁹ J.Y. Sohn,²³ A. Sokolenko,⁵⁶ E. Solodko,⁴⁵ N. Starkov,^{33,35} L. Stoel,⁴⁵ M.E. Stramaglia,⁴⁷ D. Sukhonos,⁴⁵ Y. Suzuki,²⁰ S. Takahashi,¹⁹ J.L. Tastet,³ P. Teterin,³⁹ S. Than Naing,³³ I. Timiryasov,⁴⁷ V. Tioukov,¹⁵ D. Tommasini,⁴⁵ M. Torii,²⁰ N. Tosi,¹³ D. Treille,⁴⁵ R. Tsenov,^{1,30} S. Ulin,³⁹ E. Ursov,⁴⁰ A. Ustyuzhanin,^{41,35} Z. Uteshev,³⁹ L. Uvarov,³⁷ G. Vankova-Kirilova,¹ F. Vannucci,⁵ P. Venkova,⁶ V. Venturi,⁴⁵ I. Vidulin,⁴⁰ S. Vilchinski,⁵⁶ Heinz Vincke,⁴⁵ Helmut Vincke,⁴⁵ C. Visone,^{15,d} K. Vlasik,³⁹ A. Volkov,^{33,34} R. Voronkov,³³ S. van Waasen,⁹ R. Wanke,¹⁰ P. Wertelaers,⁴⁵ O. Williams,⁴⁵ J.-K. Woo,²⁵ M. Wurm,¹⁰ S. Xella,³ D. Yilmaz,⁵⁰ A.U. Yilmazer,⁵⁰ C.S. Yoon,²³ Yu. Zaytsev,³¹ A. Zelenov³⁷ and J. Zimmerman⁶

¹Faculty of Physics, Sofia University, Sofia, Bulgaria

²Universidad Técnica Federico Santa María and Centro Científico Tecnológico de Valparaíso, Valparaíso, Chile

³Niels Bohr Institute, University of Copenhagen, Copenhagen, Denmark

*Corresponding author.

- ⁴LAL, Univ. Paris-Sud, CNRS/IN2P3, Université Paris-Saclay, Orsay, France
- ⁵LPNHE, IN2P3/CNRS, Sorbonne Université, Université Paris Diderot, F-75252 Paris, France
- ⁶Humboldt-Universität zu Berlin, Berlin, Germany
- ⁷Physikalisches Institut, University of Freiburg, Freiburg, Germany
- ⁸Universität Hamburg, Hamburg, Germany
- ⁹Forschungszentrum Jülich GmbH (KFA), Jülich, Germany
- ¹⁰Institut für Physik and PRISMA Cluster of Excellence, Johannes Gutenberg Universität Mainz, Mainz, Germany
- ¹¹Universität Siegen, Siegen, Germany
- ¹²Sezione INFN di Bari, Bari, Italy
- ¹³Sezione INFN di Bologna, Bologna, Italy
- ¹⁴Sezione INFN di Cagliari, Cagliari, Italy
- ¹⁵Sezione INFN di Napoli, Napoli, Italy
- ¹⁶Laboratori Nazionali dell'INFN di Frascati, Frascati, Italy
- ¹⁷Laboratori Nazionali dell'INFN di Gran Sasso, L'Aquila, Italy
- ¹⁸Aichi University of Education, Kariya, Japan
- ¹⁹Kobe University, Kobe, Japan
- ²⁰Nagoya University, Nagoya, Japan
- ²¹College of Industrial Technology, Nihon University, Narashino, Japan
- ²²Toho University, Funabashi, Chiba, Japan
- ²³Physics Education Department & RINS, Gyeongsang National University, Jinju, Korea
- ²⁴Gwangju National University of Education,^e Gwangju, Korea
- ²⁵Jeju National University,^e Jeju, Korea
- ²⁶Korea University, Seoul, Korea
- ²⁷Sungkyunkwan University,^e Suwon-si, Gyeong Gi-do, Korea
- ²⁸University of Leiden, Leiden, The Netherlands
- ²⁹LIP, Laboratory of Instrumentation and Experimental Particle Physics, Portugal
- ³⁰Joint Institute for Nuclear Research (JINR), Dubna, Russia
- ³¹Institute of Theoretical and Experimental Physics (ITEP) NRC “Kurchatov Institute”, Moscow, Russia
- ³²Institute for Nuclear Research of the Russian Academy of Sciences (INR RAS), Moscow, Russia
- ³³P.N. Lebedev Physical Institute (LPI RAS), Moscow, Russia
- ³⁴National Research Centre “Kurchatov Institute”, Moscow, Russia
- ³⁵National University of Science and Technology “MISiS”, Moscow, Russia
- ³⁶Institute for High Energy Physics (IHEP) NRC “Kurchatov Institute”, Protvino, Russia
- ³⁷Petersburg Nuclear Physics Institute (PNPI) NRC “Kurchatov Institute”, Gatchina, Russia
- ³⁸St. Petersburg Polytechnic University (SPbPU),^f St. Petersburg, Russia
- ³⁹National Research Nuclear University (MEPhI), Moscow, Russia
- ⁴⁰Skobeltsyn Institute of Nuclear Physics of Moscow State University (SINP MSU), Moscow, Russia
- ⁴¹Yandex School of Data Analysis, Moscow, Russia
- ⁴²Institute of Physics, University of Belgrade, Serbia
- ⁴³Stockholm University, Stockholm, Sweden
- ⁴⁴Uppsala University, Uppsala, Sweden
- ⁴⁵European Organization for Nuclear Research (CERN), Geneva, Switzerland
- ⁴⁶University of Geneva, Geneva, Switzerland

⁴⁷ *École Polytechnique Fédérale de Lausanne (EPFL), Lausanne, Switzerland*

⁴⁸ *Physik-Institut, Universität Zürich, Zürich, Switzerland*

⁴⁹ *Middle East Technical University (METU), Ankara, Turkey*

⁵⁰ *Ankara University, Ankara, Turkey*

⁵¹ *H.H. Wills Physics Laboratory, University of Bristol, Bristol, United Kingdom*

⁵² *STFC Rutherford Appleton Laboratory, Didcot, United Kingdom*

⁵³ *Imperial College London, London, United Kingdom*

⁵⁴ *University College London, London, United Kingdom*

⁵⁵ *University of Warwick, Warwick, United Kingdom*

⁵⁶ *Taras Shevchenko National University of Kyiv, Kyiv, Ukraine*

^a *Università di Bari, Bari, Italy*

^b *Università di Bologna, Bologna, Italy*

^c *Università di Cagliari, Cagliari, Italy*

^d *Università di Napoli “Federico II”, Napoli, Italy*

^e *Associated to Gyeongsang National University, Jinju, Korea*

^f *Associated to Petersburg Nuclear Physics Institute (PNPI), Gatchina, Russia*

^g *Also at Moscow Institute of Physics and Technology (MIPT), Moscow Region, Russia*

^h *Consorzio CREATE, Napoli, Italy*

ⁱ *Università della Basilicata, Potenza, Italy*

^j *Università di Napoli Parthenope, Napoli, Italy*

E-mail: markus.cristinziani@uni-siegen.de,

nikolaus.owtscharenko@uni-siegen.de

ABSTRACT: In July 2018 an optimization run for the proposed charm cross section measurement for SHiP was performed at the CERN SPS. A heavy, moving target instrumented with nuclear emulsion films followed by a silicon pixel tracker was installed in front of the Goliath magnet at the H4 proton beam-line. Behind the magnet, scintillating-fibre, drift-tube and RPC detectors were placed. The purpose of this run was to validate the measurement’s feasibility, to develop the required analysis tools and fine-tune the detector layout. In this paper, we present the track reconstruction in the pixel tracker and the track matching with the moving emulsion detector. The pixel detector performed as expected and it is shown that, after proper alignment, a vertex matching rate of 87% is achieved.

KEYWORDS: Particle tracking detectors (Solid-state detectors); Pattern recognition, cluster finding, calibration and fitting methods; Detector alignment and calibration methods (lasers, sources, particle-beams)

ARXIV EPRINT: [2112.11754](https://arxiv.org/abs/2112.11754)

Contents

1	Introduction	1
2	Experimental setup	2
2.1	Beam conditions and data taking	2
2.2	Pixel detector	3
3	Track finding and reconstruction	4
3.1	Emulsion detector	4
3.2	Pixel detector	4
3.3	Alignment and track matching procedure	5
4	Results	6
4.1	Track matching	6
4.2	Physics performance	7
5	Conclusion	8

1 Introduction

Knowledge of the charm production cross section in a thick target is of key importance for the proposed SHiP [1] experiment. The prediction of charmed-hadron production is essential to establish the sensitivity to detect new particles and to make a precise estimate of the ν_τ flux stemming from charm decays. Current information on charm production at a center-of-mass energy of $\sqrt{s} = 27$ GeV is limited to measurements with thin targets [2]. For the determination of the flux of charmed hadrons the cascade production is of crucial importance and needs to be verified experimentally. The SHiP-charm project [3] aims at measuring the double-differential cross section, $d^2\sigma/(dE d\theta)$, for charm production using the 400 GeV/ c primary proton beam, extracted from SPS to the H4 beam-line of the SPS North Area at CERN. The target consisted of a shorter replica of the SHiP SND detector, and is interleaved with emulsion cloud chambers (ECC) for tracking charm production and decays. This was followed by a magnetized tracking spectrometer and by a muon tagger. In July 2018, an optimization run took place at the H4 beam-line. We address the challenge of reconstructing common tracks (and events) from the information recorded by the fundamentally different ECC and pixel detectors. This is complicated by the fact that the ECC detector carries no timing information and was moving relative to the beam and the pixel detector in order to prevent overexposure during a given spill. In this paper, results of matching ECC tracks and vertices to downstream pixel tracks by means of a χ^2 minimization of the residuals are presented.

2 Experimental setup

The experiment was composed of three major parts: the ECC, the spectrometer and a muon tagger. For the measurement, 400 GeV/ c protons impinging on the ECC, made of tungsten sheets alternated with nuclear emulsion films. A detailed description of the ECC can be found in [4]. The most important properties are a very high spatial resolution and the permanence of each ionization trace. The permanent ionization makes it necessary to limit the occupancy in the emulsion films. The first electronic detector, 1.8 cm downstream of the ECC, was the pixel detector. It was the first of three sub-detectors building the spectrometer together with GOLIATH [5, 6]. Downstream of the magnet, a scintillating-fiber (SciFi) tracker of 40 cm \times 40 cm area per plane was positioned. It was followed by a drift-tube detector [7], covering the outer regions of acceptance. The last detector was the muon tagger, built from resistive-plate chambers (RPCs) and an iron filter. Figure 1 displays the setup along the beam axis. Since the linking of analog ECC information with the pixel-detector tracks is crucial to the overall reconstruction and event selection, this paper focuses on this critical step. For the analysis described below, only the stand-alone data of these two detectors is used. While the ECC is passive, the pixel detector was triggered by the beam counter, a pair of scintillators requiring coincident detection of the primary beam protons.

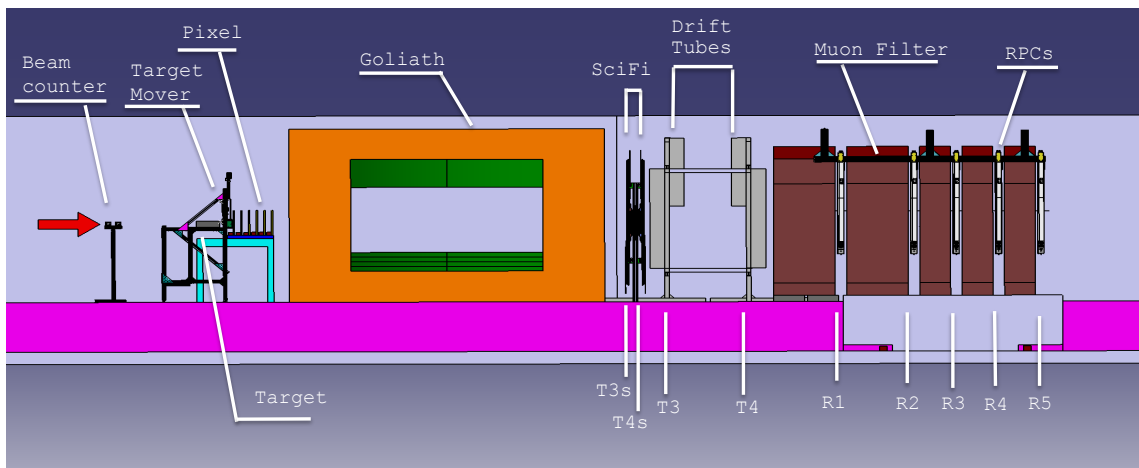


Figure 1. Conceptual drawing of the SHiP-charm experiment setup for the 2018 test beam [4]. The ECC is referred to as “target”.

2.1 Beam conditions and data taking

The beam in the North Area (and H4 beam-line) is slowly extracted in spills of mostly uniform duration of ~ 4.8 s. The beam was tuned to an elliptical shape with an extent of approximately 2 cm in y and 0.7 cm in x .¹ The number of protons per spill ranged from 7700 to 13 800. The occupancy limit on the ECC made it necessary to move the detector through the beam, and the beam shape was chosen to maximize the illuminated active area in this setup. The pixel detector was

¹The coordinate system is defined such that the z -axis is parallel to the beam-line, the positive y -axis points upwards, while positive x points to the right (direction “Salève”) when looking downstream of the beam. The most downstream emulsion layer is located at $z = 0$.

synchronized via the analog start-of-spill signal, which was used to reset trigger counters and/or timestamps before each spill. The trigger counts all incoming protons and every trigger creates a new event. Different target configurations were used for the SHiP-charm test-beam [4]. For this work one dedicated configuration is considered where the target consisted of 29 emulsion films interleaved with 28 tungsten sheets, adding up to a total passive-material budget of 2.5 cm within the 5 cm thick ECC. In this configuration the occupancy on the pixel detector for events with proton interaction was on average 86 cluster per plane per event, creating a high-occupancy environment for track reconstruction. Figure 2 shows the number of cluster per event for the single detector planes. During each of the five spills, the target moved at about ± 2.6 cm/s along the horizontal axis, inverting the direction with every new spill. In between spills it was shifted upwards by 2 cm, forming a snake-like pattern.

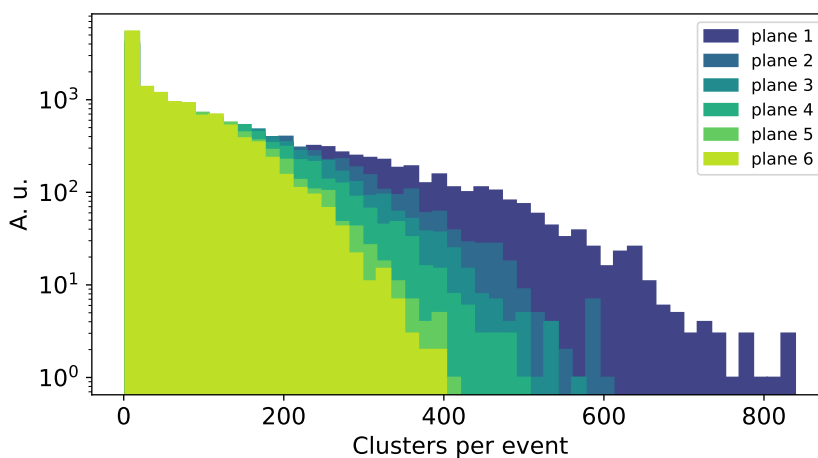


Figure 2. Overlay of histograms of the number of clusters per event in events with a proton interaction for all detector planes. The average for the most downstream plane 1 is 134 cluster per event with a maximum of 838.

2.2 Pixel detector

As the most upstream element of the spectrometer, the pixel detector connects the analog information of the ECC with data taken by the other electronic sub-detectors: the ionization in the ECC is permanent, without any timing information. Tracks reconstructed in the pixel detector provide the necessary timestamp to fully reconstruct the event.

The pixel tracking detector consisted of six planes, each formed by two ATLAS IBL double-chip modules with hybrid pixels [8]. ATLAS hybrid pixel detectors consist of a pixelated silicon sensor and the FE-I4 read-out chip. The front-end chip offers an analog readout for every sensor pixel. They are electrically connected via solder bumps. Sensor and read-out chip were developed for a high-radiation and high-occupancy environment. The FE-I4 clock runs at 40 MHz which is therefore the maximum timing resolution.

One double-chip module is organized in 160 columns and 336 rows, resulting in 53 760 pixels. The pixel pitch for the rows is 50 μm , and 250 μm for the columns. Pixels in the two central columns are 450 μm wide to compensate for the small but necessary gap between the two independent

front-end chips. To maximize the active area, edge columns are also wider, 500 μm , with partially overlapping guard rings on the sensor. A double-chip sensor measures 4.09 cm \times 1.68 cm, resulting in an active area of about 6.9 cm². The sensors are about 200 μm thick and were biased with -80 V. The sensor's hit detection efficiency is above 99 % [9]. The front-end chips were tuned to a threshold corresponding to about 1600 e^- .

The detector layout was optimized to achieve the best possible pointing resolution towards the ECC. The difference in pixel resolution between the x and y dimensions was compensated by rotating every other plane by $\pi/2$ around the beam axis. This layout allows for three high resolution measurements in each dimension, x and y , starting with 50 μm resolution in x on the first plane. Furthermore, the mounting and position of the planes relative to each other was optimized for maximal acceptance. To create a plane, two modules are placed on opposite sides of a single aluminium frame. This layout allows for a continuous active area. The aluminium frames were cut out to reduce the material budget as much as possible, while retaining the required mechanical stability and thermal contact.

3 Track finding and reconstruction

In the following we briefly discuss the independent track reconstruction in the ECC and the pixel detector, the alignment of the two detector systems with respect to each other and finally the matching of common tracks.

3.1 Emulsion detector

Track reconstruction within the ECC is performed in two steps. First the emulsion films are scanned under a microscope to digitize the tracklets, second tracks are reconstructed from the tracklets with the FEDRA software [10]. The intrinsic resolution of the emulsion films is 0.7 μm [11] and the average film-by-film track efficiency was measured to be (92 ± 2) % [4]. The reconstructed tracks contain a set of at least two track segments, one for each emulsion plane. For track finding and fitting, a Kalman-Filter algorithm is used, taking into account inefficiencies in the reconstruction of track segments [11]. The track reconstruction purity was measured to be above 95 % [12]. Two-track vertices are identified with a criterion on the distance-of-closest-approach. They are associated to a common vertex based on a vertex probability taking into account the full covariance matrix of all involved tracks. Detailed information regarding the reconstruction is available in reference [4].

3.2 Pixel detector

Tracks in the pixel detector are reconstructed with a local pattern recognition starting from a track seed formed by two hits on the third and last detector plane. Track candidates are validated with a χ^2 minimization fit. The pattern recognition only considers tracks with opening angles $\theta_{xz}, \theta_{yz} \leq 150$ mrad, matching the spectrometer acceptance. A detailed description of the reconstruction can be found in [13]. For the investigated run, 36 132 events from 5 spills were recorded. The pixel detector efficiency is between 99.5 and 99.9 %, while the tracking resolution is found to be 15 μm in x and 26 μm in y direction [13].

3.3 Alignment and track matching procedure

In order to match track candidates between the pixel and the moving emulsion detectors, a set of good track candidates is selected and used for a proper alignment. First, emulsion tracks are selected if they are associated to a vertex with at least six associated tracks. Tracks also have to feature a segment in the most downstream emulsion layer. To minimize the influence of multiple scattering on the track resolution, only the track parameters of that most downstream segment are used in the following. In order to suppress tracks from fully penetrating protons (i.e., the beam), the number of track segments per track must be less than 29 (the total number of segments).

The track parameters of interest for matching are the positions x , y and the track angles θ_x and θ_y of the furthest downstream track segment. The track angles θ_x and θ_y are required to be less than 150 mrad each, in order only consider tracks within the spectrometer acceptance. The time information provided with each reconstructed pixel detector track, $t = \text{timestamp} \times 25 \text{ ns}$, is used to translate the pixel detector's local coordinate system into the moving emulsion frame and transform the pixel track parameters $\mathbf{x}^{\text{pix}} = (x, y, z, \theta_x, \theta_y)$, accordingly. The uncertainty in the time t is $\mathcal{O}(\text{ns})$, which is small compared to the overall uncertainty coming from the spread in x and the speed of the target mover $\mathcal{O}(\text{ms})$, and is thus negligible.

For the alignment, a set of eight parameters is introduced, $\boldsymbol{\alpha} = (x_0, y_0, z_0, \theta_{xz}, \theta_{yz}, \theta_{xy}, v_x, v_y)$, where x_0, y_0, z_0 are the offset of the pixel detector with respect to the emulsion reference frame, the two velocities v_x and v_y characterize the target mover, and the rotations of the pixel detector about the x , y , and z axes are denoted by θ_{yz} , θ_{xz} and θ_{xy} , respectively. The origin is set at the most downstream emulsion layer. We define a track χ_{track}^2 of residuals between the emulsion and pixel detectors as

$$\chi_{\text{track}}^2 = \mathbf{r}^T \mathbf{V}^{-1} \mathbf{r}, \quad (3.1)$$

where $\mathbf{r} = \mathbf{x}^{\text{pix}} - \mathbf{x}^{\text{ECC}} = (\Delta x, \Delta y, \Delta \theta_x, \Delta \theta_y)$ is the vector of residuals and $\mathbf{V} = \mathbf{V}^{\text{pix}} + \mathbf{V}^{\text{ECC}}$ is the covariance matrix of residuals evaluated at the matching plane of $z = 0$. The list of good track matches is constructed by calculating the χ^2 of every possible pair between emulsion and pixel tracks. Only pairs with a $\chi^2 < 100$ are considered. Furthermore, there is a requirement on residuals of $\pm 5 \text{ mm}$ in Δx , and Δy and a $\pm 15 \text{ mrad}$ cut on the residuals in $\Delta \theta_x$, and $\Delta \theta_y$. The list is then ordered in increasing values of χ^2 . A new list is created by starting from the beginning (smallest χ^2) and moving down the list, at each step checking whether either the emulsion or pixel track were already used, in which case the pair would be removed from the list. This creates a set of good track matches with the minimal χ^2 for a given set of alignment parameters. Whether this is the best possible list (minimal χ^2) will depend on whether the two sub-detectors are properly aligned. The total

$$\chi^2 = \sum_j (\mathbf{r}^T \mathbf{V}^{-1} \mathbf{r})_j, \quad (3.2)$$

is to be minimized, where the sum runs over track pairs j between the emulsion and pixel tracks [14]. The condition that the sample of tracks is minimal with respect to the alignment parameters can be written as

$$0 \equiv \frac{d\chi^2}{d\boldsymbol{\alpha}} = 2 \sum_j \left(\frac{\partial \mathbf{r}^T}{\partial \boldsymbol{\alpha}} \mathbf{V}^{-1} \mathbf{r} \right)_j. \quad (3.3)$$

The optimal value of α that satisfies this relation can be determined using the Newton-Raphson method. Given an initial set of alignment parameters α_0 , an updated set α_1 is calculated as

$$\alpha_1 = \alpha_0 - \left(\frac{d^2\chi^2}{d\alpha^2} \right)^{-1} \bigg|_{\alpha_0} \left(\frac{d\chi^2}{d\alpha} \right) \bigg|_{\alpha_0}. \quad (3.4)$$

This step is iterated until a convergence criterion is met, namely a minimal change in χ^2 with increasing iterations. The alignment procedure can be summarized as follows:

1. Begin with an initial set of alignment parameters α_0 .
2. Calculate the χ^2 per track pair with eq. (3.1) and find the list of pairs with the minimal χ^2 .
3. Calculate the total χ^2 using eq. (3.2).
4. Get a new set of alignment parameters α_1 using eq. (3.4).
5. Go back to Step 2 using α_1 in place of α_0 and repeat until the total χ^2 converges.

Convergence of the χ^2 is not necessarily assured. If the misalignment is too large, the optimal set of track pairs could have a χ^2 so large that it is dominated by combinatorial background, i.e., a pair with a large χ^2 could take the place of an actual match if they share a track. Therefore, it is important to begin with a set of alignment parameters that are close to the optimal values.

4 Results

4.1 Track matching

The alignment and matching procedure was performed on the data, where each spill was treated separately. Some alignment parameters are constrained by the initial mechanical alignment in the cavern before data taking, in particular the SHiP-charm setup was surveyed by the CERN EN/SMM group [15]. The distance between the last emulsion layer and the first pixel layer was measured to be $z_0 = (1.8 \pm 0.1)$ cm while the speed of the target mover in the horizontal direction was measured to be $v_x = (2.6 \pm 0.1)$ cm/s. The value of y_0 changed depending on the spill and is estimated from the beam profile in y . The angles θ_{xz} , θ_{yz} and θ_{xy} and the target mover speed in the vertical direction v_y are initially set to 0. The alignment parameter x_0 is initially unknown, but can be estimated by setting $\Delta x = 0$ in the χ^2 calculation and then looking for a peak in the resulting Δx distribution after alignment.

The evolution of the mean χ^2 of all tracks is shown in figure 3, illustrating the improvement in the χ^2 after alignment. The matching resolutions are found to be $\sigma_x = 44 \mu\text{m}$, $\sigma_y = 80 \mu\text{m}$, $\sigma_{\theta_{xz}} = 4 \text{ mrad}$, and $\sigma_{\theta_{yz}} = 3 \text{ mrad}$.

A shift in x_0 of about 13.7 cm between alternate spills corresponds to the target moving $v_x \sim 2.6$ cm/s for 5.2 s, closely matching the target moving time, which included 0.4 s before/after the spill. Likewise, an observed shift in y_0 between spills can be explained by a vertical movement of $v_y \sim 300 \mu\text{m/s}$. The distance between the last emulsion layer and first pixel layer z_0 is consistent with the survey measurement [15]. The angles θ_{xz} and θ_{yz} are close to 0, while θ_{xy} is about 19 mrad. Since v_y changes sign between spills, this vertical velocity corresponds to a rotation of the emulsion brick with respect to the beam of about 11 mrad.

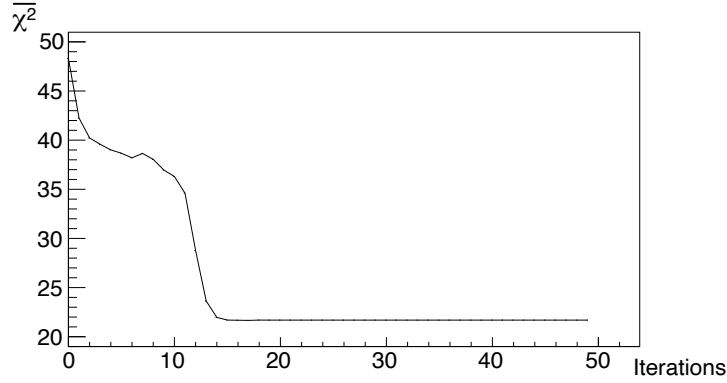


Figure 3. The average χ^2 per track vs. the number of iterations of the alignment procedure.

4.2 Physics performance

For the investigation of charmed hadronic interaction in SHiP-charm, a full event reconstruction including particle identification is necessary. This was achieved by measuring track deflection downstream of the magnetic field. Thus, the current analysis is focused on tracks which stay within the experiments acceptance and characteristic events are selected considering two main features.

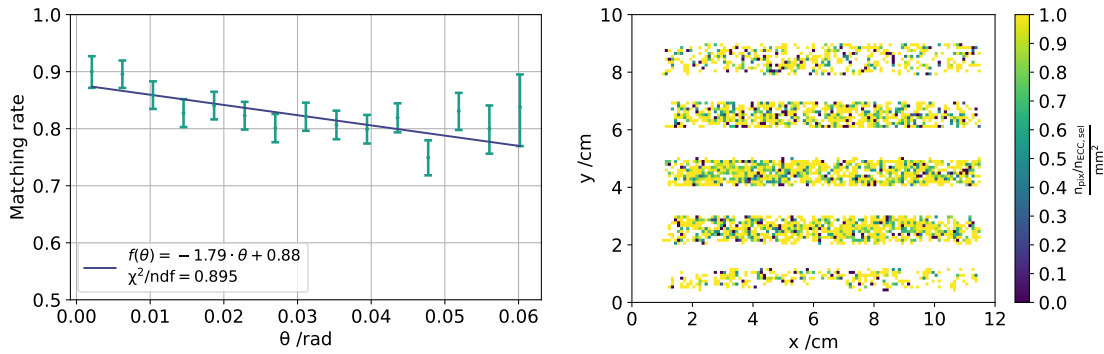


Figure 4. Track matching rate in the connected sub-detectors vs. track angle θ (left) and vs. x and y position of selected tracks (right). The non-uniform distribution of horizontal lines reflects the single spills.

In a first step only tracks from vertices with at least six tracks reconstructed in the ECC are selected. Secondly, the magnetic deflection of tracks beyond the SciFi detectors' acceptance is considered, and only tracks with opening angles smaller than 62 mrad are selected. The detector performance is then quantified in terms of the matching rate ϵ . Given a set of n tracks, the matching rate is defined as the ratio of the number of ECC tracks matched in the pixel detector n_{pix} over the number of selected ECC tracks $n_{\text{ECC,sel}}$:

$$\epsilon = \frac{n_{\text{pix}}}{n_{\text{ECC,sel}}}.$$

In figure 4 the matching rate distributions for track matching after this selection are shown for the entire run. The average matching rate for selected emulsion tracks is $(82.6 \pm 0.4)\%$. With the

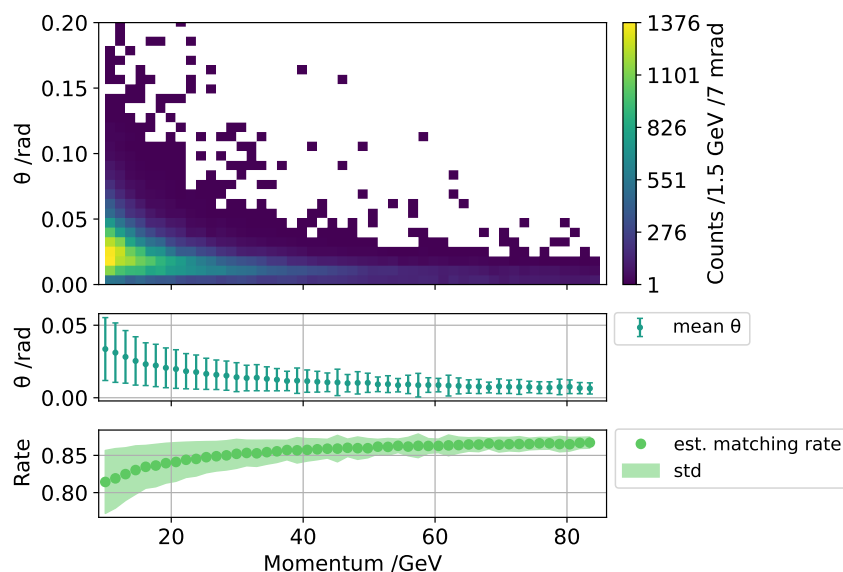


Figure 5. Track angle (top), average angle (center) and estimated matching rate (bottom) vs. momentum of Monte Carlo tracks in the emulsion. Only tracks within the experiments acceptance are considered.

successful matching of at least one track a timestamp is assigned not only to the track but to the whole vertex. Thus, after matching, timestamps can be assigned to 87 % of selected vertices. If a vertex is assigned a timestamp, the matching rate for tracks of this vertex is at least 88 % on average, while for 65 % of matched vertices all selected tracks are matched.

The relation between track angle and matching rate can be used to estimate a matching rate with respect to the particles' momentum. In figure 4 (left) the rate is plotted for different track angles and a fit is performed. The uncertainties are computed by quadratic addition of the statistical uncertainty and the estimated systematic uncertainty. The statistical uncertainty is computed as the $1\text{-}\sigma$ confidence interval of a binomial distribution, according to Bayes' theorem [16, 17]. The systematic uncertainty is determined using the mean difference of the matching rate for varying χ^2 constraints. The fitted model is applied to the average track angle for given momenta as obtained from a Monte-Carlo simulation of particle interactions in the ECC [4]. Tracks with $p < 10$ GeV are not considered, as these tracks are leaving the experimental setup after magnetic deflection. The result is plotted in figure 5. For all tracks within the detector acceptance we expect a matching rate of at least 81 %, increasing to 87 % with track momentum.

5 Conclusion

In this paper it is demonstrated that a moving emulsion detector without timing information and a stationary high-granularity pixel detector can successfully be used for track reconstruction in a high occupancy environment. The Newton-Raphson method is used to determine a set of eight alignment parameters. Two aspects were crucial for a successful alignment, a small distance between the two detectors and a set of adequate parameters to start the alignment procedure. With the described algorithm, 82.6 % of the emulsion tracks within detector acceptance can be matched, corresponding

to 87 % of characteristic vertices. This proves the combination of ECC and pixel detector as well suited for a charm cross section measurement in the given setup. To evaluate whether the physics program can be met, a second optimization run and a study employing the whole spectrometer would be necessary.

Acknowledgments

The SHiP Collaboration acknowledges support from the National Research Foundation of Korea, the Fundação para a Ciência e a Tecnologia of Portugal, FCT; the Russian Foundation for Basic Research, RFBR and the TAEK of Turkey. This work is supported by the German Science Foundation (DFG) through a research grant and a Heisenberg professorship under contracts CR-312/4-1 and CR-312/5-1. We thank W. Dietsche, F. Hüggling, J. Janssen and D.L. Pohl of SILAB, Bonn for their assistance with the pixel detector. The measurement reported in this paper would not have been possible without a significant financial contribution from CERN. In addition, several member institutes made large financial and in-kind contributions to the construction of the target and the spectrometer sub-detectors, as well as providing expert manpower for commissioning, data taking and analysis. This help is gratefully acknowledged.

References

- [1] SHiP collaboration, *A facility to Search for Hidden Particles (SHiP) at the CERN SPS*, Tech. Rep., [CERN-SPSC-2015-016](#), CERN, Geneva (2015) [[arXiv:1504.04956](#)].
- [2] C. Lourenço and H.K. Wöhri, *Heavy flavour hadro-production from fixed-target to collider energies*, *Phys. Rept.* **433** (2006) 127 [[hep-ph/0609101](#)].
- [3] SHiP collaboration, *Measurement of associated charm production induced by 400 GeV/c protons*, Tech. Rep., [CERN-SPSC-2017-033](#), CERN, Geneva (2017).
- [4] SHiP collaboration, *Reconstruction of 400 GeV/c proton interactions with the SHiP-charm project*, Tech. Rep., [CERN-SHiP-NOTE-2020-002](#), CERN, Geneva (2020).
- [5] Y. Gaillard, *Specification technique concernant la refexion de l'electro-aimant Goliath*, Tech. Rep., EDMS 1326984, CERN, Geneva (1969).
- [6] M. Rosenthal et al., *Magnetic Field Measurements of the GOLIATH Magnet in EHN1*, Tech. Rep., [CERN-ACC-NOTE-2018-0028](#), CERN, Geneva (2018).
- [7] R. Zimmermann, J. Ebert, C. Hagner, B. Koppitz, V. Savelev, W. Schmidt-Parzefall et al., *The precision tracker of the OPERA detector*, *Nucl. Instrum. Meth. A* **555** (2005) 435 [*Erratum ibid.* **557** (2006) 690]
- [8] ATLAS IBL collaboration, *Production and Integration of the ATLAS Insertable B-Layer*, [2018 JINST 13 T05008](#) [[arXiv:1803.00844](#)].
- [9] ATLAS IBL collaboration, *Prototype ATLAS IBL Modules using the FE-I4A Front-End Readout Chip*, [2012 JINST 7 P11010](#) [[arXiv:1209.1906](#)].
- [10] V. Tioukov, I. Kreslo, Y. Petukhov and G. Sirri, *The FEDRA Framework for emulsion data reconstruction and analysis in the OPERA experiment*, *Nucl. Instrum. Meth. A* **559** (2006) 103.
- [11] L. Arrabito et al., *Track reconstruction in the emulsion-lead target of the OPERA experiment using the ESS microscope*, [2007 JINST 2 P05004](#) [[arXiv:0705.3102](#)].

- [12] A. Iuliano, *Event reconstruction and data analysis techniques for the SHiP experiment*, Ph.D. Thesis, Università degli Studi di Napoli Federico II, (2021) [<https://cds.cern.ch/record/2776128/files/CERN-THESIS-2021-091.pdf>]
- [13] SHiP collaboration, *Track reconstruction and matching for SHiP-charm*, Tech. Rep., [CERN-SHiP-NOTE-2020-003](#), CERN, Geneva (2020).
- [14] A. Bocci and W. Hulsbergen, *TRT alignment for SR1 cosmics and beyond*, Tech. Rep., [ATL-INDET-PUB-2007-009](#), CERN, Geneva (2007).
- [15] B. Cumer and K. Nikolitsas, *H4 test measurement of the charm cross section setup on H4 beam line*, Tech. Rep., [EDMS 2010858](#), CERN, Geneva (2018).
- [16] D. Casadei, *Estimating the selection efficiency*, [2012 JINST 7 P08021](#) [[arXiv:0908.0130](#)].
- [17] M. Paterno, *Calculating Efficiencies and Their Uncertainties*, Tech. Rep., [FERMILAB-TM-2286-CD](#), Fermilab, Batavia, IL, U.S.A. (2004).